Dyes and Pigments 184 (2021) 108652

Contents lists available at ScienceDirect

Dyes and Pigments

journal homepage: http://www.elsevier.com/locate/dyepig

Dynamic dye emission ON/OFF systems by a furan moiety exchange protocol

Qi Zhang, Ying Wang [**], Junbo Gong [***], Xin Zhang [*]

School of Chemical Engineering and Technology, Collaborative Innovation Center of Chemistry Science and Engineering, Tianjin University, Tianjin, 300072, China

ARTICLE INFO

Keywords:
Dynamic covalent chemistry
Triphenylamines
Fluorescence
Supramolecular assembly

ABSTRACT

Four triphenylamine-based dyes were synthesized by fluorescence turn on reactions. Optical behaviours, molecular arrangements, donor-to-acceptor charge transfer and dipole interactions of these functional dyes were investigated by UV–vis absorption and fluorescence spectroscopy, single-crystal X-ray diffraction and electrochemical cyclic voltammetry. The irreversible isomerization of itaconimide dye leads to an irreversible emission switch ON to OFF. Reversible Diels-Alder reaction of these dyes lead to a reversible emission switch OFF/ON. These luminescent dyes demonstrate dynamic dye molecular features by furan moiety exchanges to form energy-minimized and optimized dye molecular structures. In the dynamic molecular system, α-position furan-substituted dye was converted into more stable β-position furan-substituted dye according to ^{1}H NMR spectroscopic monitoring.

1. Introduction

Reversible cleavage and reformation of covalent bonds are the most interesting features of dynamic covalent reaction, which allow the exchange of molecular moieties at equilibrium to achieve thermodynamic minimum of system [1–5]. Compared with supramolecular weak non-covalent bonds [6–9], dynamic covalent bonds are more robust with response for the environments including temperature, light, mechanical stress, magnetic and electrical fields [10–12]. By dynamic covalent reactions, chemists have prepared a wide range of fascinating 1D, 2D and 3D molecular architectures such as polymers [13,14], molecular knots [15], covalent organic frameworks [16–20], and macrocycles [21,22]. Dynamic covalent reactions can be classified into two main reactions, i.e. exchange reactions including ester, disulfide, furan, amine and acetal exchanges, and new dynamic covalent bond formation reactions including aldol reaction, imine condensation and cycloadditions. On the basis of above outstanding dynamic properties, dynamic covalent dye chemistry has shown various applications such as self-healing, renewable and recyclable materials [23–25], chemical sensors [26,27], biomedical [28], gas storage [29,30]. Recently, Zhang and Jin et al. elegantly described recyclable plastics and thermosets based on dynamic covalent bonds [31]. Ji et al. reported self-healable, recyclable, reprocessable liquid crystalline epoxy thermosets and elastomers with dynamic covalent bonds [32]. Summerlin et al. utilized the reversible properties of Diels-Alder reaction to prepare smart materials with morphology transitions [33].

A very interesting class of dynamic covalent reactions is the Diels-Alder [4 + 2] cycloaddition of electron-rich dienes and electron-poor dienophile [34,35]. Diels-Alder furan-maleimide addition reaction can occur at ambient temperature through relatively low activation barriers, which leads to the only slightly exergonic adducts relative to starting compounds, thus allowing the *retro*-Diels-Alder addition to occur under appropriate conditions. The controllable characteristics for forward and reverse reactivity of furan-maleimide addition enable chemists to create dynamic molecular systems. In this work, we have designed and synthesized four triphenylamine-based dyes. Triphenylamine chromophores were chosen due to their propeller-like molecular structures and functional electron-donating properties for organic photoelectric p-type materials [36–38]. A high quality crystal was obtained, and its single crystal X-ray diffraction reveals the supramolecular assembling structures. The optical properties of these dyes were investigated. In particular, we demonstrate dynamic dye systems with switchable ON/OFF fluorescence behaviours.

* Corresponding author.
** Corresponding author.
*** Corresponding author.
E-mail addresses: yingwang@tju.edu.cn (Y. Wang), junbo_gong@tju.edu.cn (J. Gong), xzhangchem@tju.edu.cn (X. Zhang).

https://doi.org/10.1016/j.dyepig.2020.108652
Received 20 April 2020; Received in revised form 16 June 2020; Accepted 16 June 2020
Available online 14 August 2020

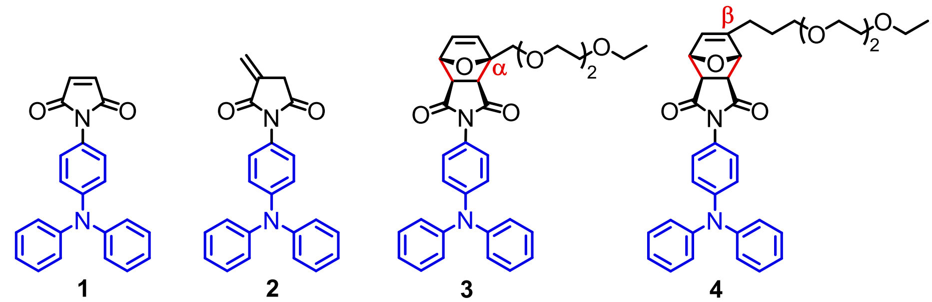

Fig. 1. Chemical structures of triphenylamine-based dyes **1** and **2** and Diels-Alder adducts **3** and **4.** Dynamic Diels-Alder bonds are indicated in red, and triphenylamine chromophores are indicated in blue. (For interpretation of the references to colour in this figure legend, the reader is referred to the Web version of this article.)

2. Experimental

2.1. Synthesis

1-(4-(diphenylamino)phenyl)-maleimide (Dye **1**) was synthesized according to the previously reported procedure [39].

1-(4-(diphenylamino)phenyl)-itaconimide (Dye 2): Itaconic anhydride (0.56 g, 5 mmol) and acetone (10 mL) were added to a 100 mL flask, and the solution was heated to 50 °C. An acetone solution (8 mL) of 4-aminotriphenylamine (0.98 g, 3.5 mmol) was added dropwise to the reaction flask, and the mixture was reacted at 50 °C for 2 h. The reaction mixture was filtered to give yellow precipitate. After drying under vacuum, the yellow precipitate was added to a 100 mL flask. Sodium acetate (0.42 g) and acetic anhydride (4.4 mL) were also added, the reaction mixture was heated to 80 °C for 13 h. After cooling to room temperature, the red solution was poured to deionized water (300 mL). The product was extracted by dichloromethane for three times and dried by anhydrous magnesium sulfate. The dichloromethane solution was concentrated under reduced pressure. The crude product was purified by silica gel column chromatography with dichloromethane/n-hexane (4/3, v/v) as eluent to give yellow solid (0.47 g) with a yield of 38%. **2** was recrystallized three times from hexane/dichloromethane (4/1, v/v) to yield yellow crystals. Mp: 159–160 °C. ^{1}H NMR (400 MHz, $CDCl_3$, ppm): $\delta = 3.51$ (t, $J = 2.1$, 2.4Hz, 2H, -COCH_2-), 5.74 (t, $J = 1.5$, 2.1Hz, 1H, =C*H*H), 6.48 (t, $J = 2.4$, 2.1Hz, 1H, =CH*H*), 7.07 (t, $J = 7.53$Hz, 2H, Ar*H*), 7.11–7.31 (m, 12H, Ar*H*). ^{13}C NMR (DMSO-d_6, ppm): $\delta = 33.82$, 119.8, 122.3, 123.6, 124.2, 124.5, 128.0, 129.7, 134.4, 146.9, 168.7, 147.1, 173.4. IR (KBr pellet, cm^{-1}): 516, 615, 694, 756, 831, 888, 951, 1145, 1275, 1322, 1384, 1500, 1588, 1658, 1714, 2925. HRMS (APCI, Fig. S8): *m/z* calcd for $C_{23}H_{18}N_2O_2[M+H]^+$: 355.1441; Found: 355.1444.

2-(4-(diphenylamino)phenyl)-4-((2-(2-ethoxyethoxy)ethoxy) methyl)-3a,4,7,7a-tetrahydro-1*H*-4,7-epoxyisoindole-1,3(2*H*)-dione (Dye **3**): Dye **1** (0.17 g, 0.5 mmol) and 2-{2-[2-(ethoxy)ethoxy]ethoxy} methyl-furan (0.13 g, 0.6 mmol) were dissolved in chloroform (5 mL). The reaction mixture was kept stirring for three days at room temperature. The product was washed with deionized water and extracted by dichloromethane for three times. After being concentrated, the crude product was purified by silica gel column chromatography with ethyl acetate/n-hexane (1/3, v/v) as eluent to give white solid (0.20 g) with a yield of 47%. ^{1}H NMR (400 MHz, $CDCl_3$, ppm): $\delta = 7.26$ (t, $J = 7.4$ Hz, 4H, Ar*H*), 7.15–7.02 (m, 10H, Ar*H*), 6.63 (d, $J = 5.4$ Hz, 1H, -C*H*=CH-), 6.56 (d, $J = 5.5$ Hz, 1H, –CH=C*H*-), 5.36 (s, 1H, -C*H*(OR)-), 4.30 (d, $J = 8.0$ Hz, 1H, -C*H*(R)-), 3.97 (d, $J = 8.0$ Hz, 1H, -C*H*(R)-), 3.82–3.47 (m, 10H, 5-OCH_2-), 3.10, 3.00 (dd, $J = 6.4$ Hz, 2H, -OCH_2-), 1.20 (t, $J = 6.9$ Hz, 3H,-CH_3). ^{13}C NMR ($CDCl_3$, ppm): $\delta = 175.4$, 174.0, 148.1,

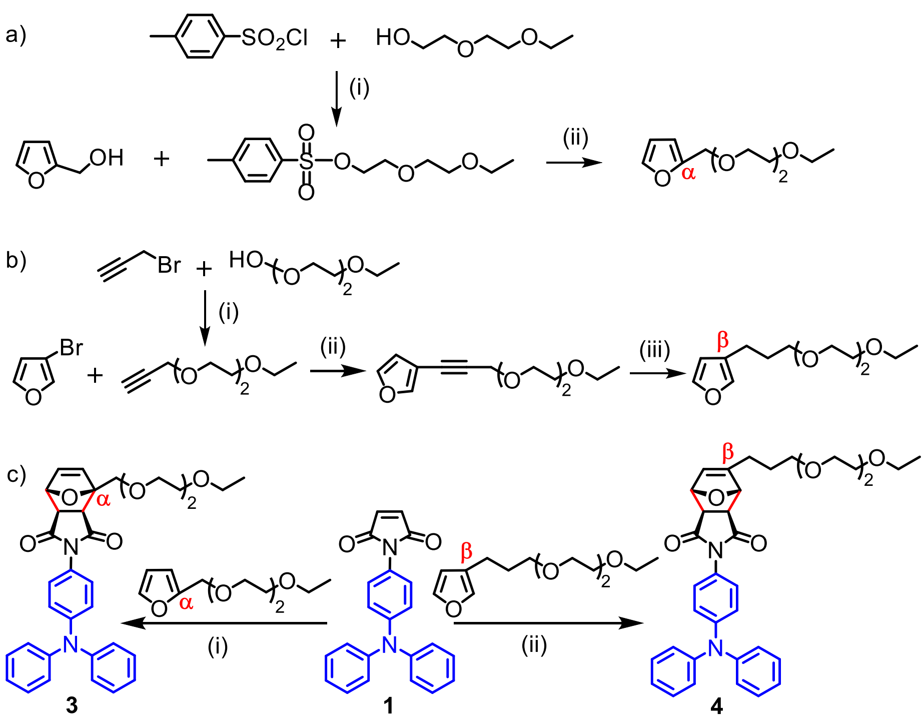

Fig. 2. a) Synthetic route toward α-position substituted furan chain. Reagents and conditions: (i) NaOH, THF/H_2O, 0 °C, 8 h, 85%; (ii) NaH, THF, 70 °C, 2 days, 74%. b) Synthetic route toward β-position substituted furan chain. Reagents and conditions: (i) Copper(I) iodide, tetrakis (triphenylphosphine) palladium, anhydrous triethylamine, 70 °C, 39%. (ii) CuI, $Pd(PPh_3)_4$, Et_3N, Ar_2, 140 °C, 6 h, 40%. (iii) Pd/C, CH_3COOH, $NaBH_4$, Ethanol, r.t., 24 h, 75%. c) Synthetic route toward dyes **3** and **4** from dye **1**. Reagents and conditions: (i) $CHCl_3$, r.t., 3 days, 47%. (ii) $CHCl_3$, r.t., 3 days, 60%.

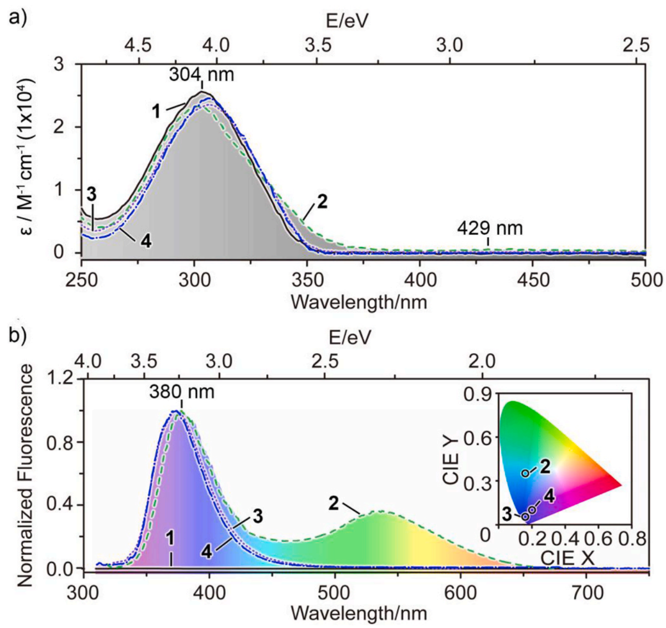

Fig. 3. a) UV–vis absorption spectra of dyes **1–4** in 1, 2-dichloroethane, $c = 5 \times 10^{-5}$ M; b) Fluorescence spectra of dyes **1–4** in 1, 2-dichloroethane, $c = 5 \times 10^{-5}$ M, $\lambda_{ex} = 310$ nm, Inset: CIE 1931 chromaticity diagram, three points are emission colour coordinates of **2** (0.16, 0.34), **3** (0.16, 0.06), **4** (0.20, 0.10)). (For interpretation of the references to colour in this figure legend, the reader is referred to the Web version of this article.)

147.3, 138.3, 136.7, 129.4, 127.2, 125.0, 123.6, 122.8, 91.0, 81.50, 71.2, 70.7, 70.4, 69.9, 68.5, 66.7, 49.9, 48.3, 15.2. IR (KBr pellet, cm^{-1}): 3462, 2968, 2924, 2870, 1776, 1709, 1589, 1508, 1489, 1385, 1317, 1281, 1190, 1100, 806, 754, 698. HRMS (ESI, Fig. S9): *m/z* calcd for $C_{33}H_{34}N_2O_6$ $[M+Na]^+$: 577.2309; Found: 577.2318.

2-(4-(diphenylamino)phenyl)-5-(3-(2-(2-ethoxyethoxy)ethoxy)propyl)-3a,4,7,7a-tetrahydro-1*H*-4,7-epoxyisoindole-1,3(2*H*)-dione (Dye **4**) was synthesized in the same manner as dye **3** except for starting materials (3-(3-{2-[2-(ethoxy)ethoxy]ethoxy}-propyl)-furan). The crude product was purified by silica gel column chromatography with ethyl acetate/n-hexane (3/2, v/v) as eluent to give white solid with a yield of 60%. ^{1}H NMR (400 MHz, $CDCl_3$, ppm): $\delta = 7.29$–7.24 (m, 5H, Ar*H*), 7.14–7.02 (m, 9H, Ar*H*), 6.08 (q, $J = 1.8$ Hz, 1H, -C*H*═C(R)-), 5.30 (s, 1H, -C*H*(OR)-), 5.13 (s, 1H, -C*H*(OR)-), 3.70–3.46 (m, 12H, -OCH_2-), 3.04 (d, $J = 8.0$ Hz, 1H, -C*H*(R)-), 2.99 (d, $J = 8.0$ Hz, 1H, -C*H*(R)-), 2.34 (t, $J = 7.6$ Hz, 2H, –CH═C(R)CH_2-), 1.88–1.73 (m, 2H, -OCH$_2$CH_2-), 1.21 (t, $J = 7.0$ Hz, 3H, -CH_3). ^{13}C NMR ($CDCl_3$, ppm): $\delta = 175.9$, 175.8, 151.9, 148.1, 147.3, 129.4, 128.7, 127.2, 125.1, 123.5, 122.8, 83.7, 82.3, 70.7, 70.6, 70.3, 70.3, 69.9, 66.7, 49.2, 47.2, 27.3, 24.1, 15.2. IR (KBr pellet, cm^{-1}): 3037, 2970, 2865, 1774, 1700, 1589, 1506, 1488, 1383, 1273, 1181, 1106, 933, 867, 750, 697. HRMS (ESI, Fig. S10): *m/z* calcd for $C_{35}H_{38}N_2NaO_6^+$ $[M+Na]^+$: 605.2622; Found: 605.2628.

3. Results and discussion

3.1. Synthesis and optical behaviours

Four triphenylamine-based dyes **1–4** (Fig. 1) were synthesized and fully characterized by NMR and IR spectroscopy and high resolution mass spectrometry (HRMS). Dyes **1** and **2** were synthesized from either maleic anhydride or itaconic anhydride, respectively via 5-member ring opening and subsequently closing reactions [40]. The precursor hydrophilic methylbenzenesulfonate chain was synthesized by the esterification reaction of tosyl chloride with diethylene glycol monoethyl ether (Fig. 2a). The α-position substituted oligo(diethylene glycol) furan chain was synthesized by nucleophilic substitution reaction from furfuryl alcohol (Fig. 2a). β-position substituted oligo(diethylene glycol) furan chain was synthesized by reduction reaction using palladium-carbon as catalyst at room temperature from corresponding alkynyl furan derivative (Fig. 2b). The alkynyl furan derivative was synthesized by the nucleophilic substitution reaction of 3-bromofuran with diethylene glycol monopropynyl ether. Dyes **3** and **4** were finally obtained by Diels-Alder [4 + 2] cycloaddition reactions of dye **1** and corresponding α- or β-position substituted oligo(diethylene glycol) furan chain without catalyst under mild conditions (Fig. 2c).

Table 1
UV–vis absorption maximum wavelength ($\lambda_{ab,\ max}$), extinction coefficient (ε), fluorescence emission maximum wavelength ($\lambda_{em,\ max}$), fluorescence quantum yields (Φ_f) and lifetimes (τ) of dyes **1–4** in 1, 2-dichloroethane.

Dyes	UV–vis absorption		Fluorescence			Stokes Shifts/ nm
	$\lambda_{ab,\ max}$/ nm	$\varepsilon/1 \times 10^4\ M^{-1}cm^{-1}$	$\lambda_{em,\ max}$/ nm	Φ_f(%)	τ/ns	
1	304	2.56	a	a	a	a
2	301, 429	2.33, 0.06	380, 537	1.81	0.81, 0.46	79, 108
3	307	2.35	374	18	0.26	67
4	307	2.46	374	24	0.28	67

[a] No fluorescence.

Dye **1** shows UV–vis absorption maximum wavelength at 304 nm with extinction coefficient ($2.56 \times 10^4\ M^{-1}cm^{-1}$) (Fig. 3a), which is assigned to π-π* transition of triphenylamine chromophore [41,42]. Dye **2** shows the π-π* transition absorption with a blue-shift of 3 nm and a slightly lower extinction coefficient. A structureless broad lower-energy absorption band at 380–520 nm was observed for dye **2**. According to Krijnen [43,44], this broad absorption band in the long-wavelength region is attributed to the lowest π-π* transition of charge transfer between triphenylamine donor and itaconimide acceptor. Dyes **3** and **4** show nearly identical absorption spectra with the same maximum wavelength at 307 nm.

These dyes show distinctly different fluorescence behaviours (Fig. 3b). Dye **1** is non-fluorescent, and the fluorescence of the triphenylamine donor is completely quenched by intramolecular charge transfer interaction with strong electron acceptor. In contrast, dye **2** is fluorescent with two emission bands (Fig. 3b). The first emission band at 380 nm is assigned to the emission of triphenylamine chromophore. For the second broad emission band at 450–650 nm, we attributed it to intramolecular charge transfer state between triphenylamine donor and itaconimide acceptor according to its absorption and excitation spectra. Dyes **3** and **4** both are fluorescent, and their fluorescence spectra are similar with the emission maximum wavelength at 374 nm. The light-emitting colour coordinates of dyes **2**, **3** and **4** are (0.16, 0.34), (0.16, 0.06) and (0.20, 0.10) within blue light region of CIE 1931 chromaticity diagram, respectively. The fluorescence quantum yields of dyes **2, 3** and **4** were measured to be 1.81%, 18% and 24%, respectively. The absorption and emission data of these dyes were listed in Table 1.

The optical and optoelectronic properties of dyes are closely related to their molecular topology 3D structures, which motivate us to explore the crystal assembly structures of triphenylamine-based dyes. The single crystal of dye **1** was prepared by slow evaporation of chloroform/dichloromethane (1/1) solution within methanol atmosphere. The crystal structure is orthorhombic system with a centrosymmetric space group of *P b c a* [45]. One unit cell consists of 8 molecules. The crystal density obtained from the X-ray diffraction is 1.275 g/cm^3. The cell length *b* of dye **1** is the nearly double the distance of lamellar stacking interval (Fig. 4b). No hydrogen bonding or π-π stacking interaction was observed in crystal packing structure. Triphenylamine chromophore adopts a propeller–like conformation (Fig. 4a). In crystal structure, the dye molecules are assembled in an alternating donor-acceptor head-to-tail manner (Fig. 4b, c, d). Thus, the main driving force for the formation of packing structure of dye **1** is the donor-accepter dipole-dipole

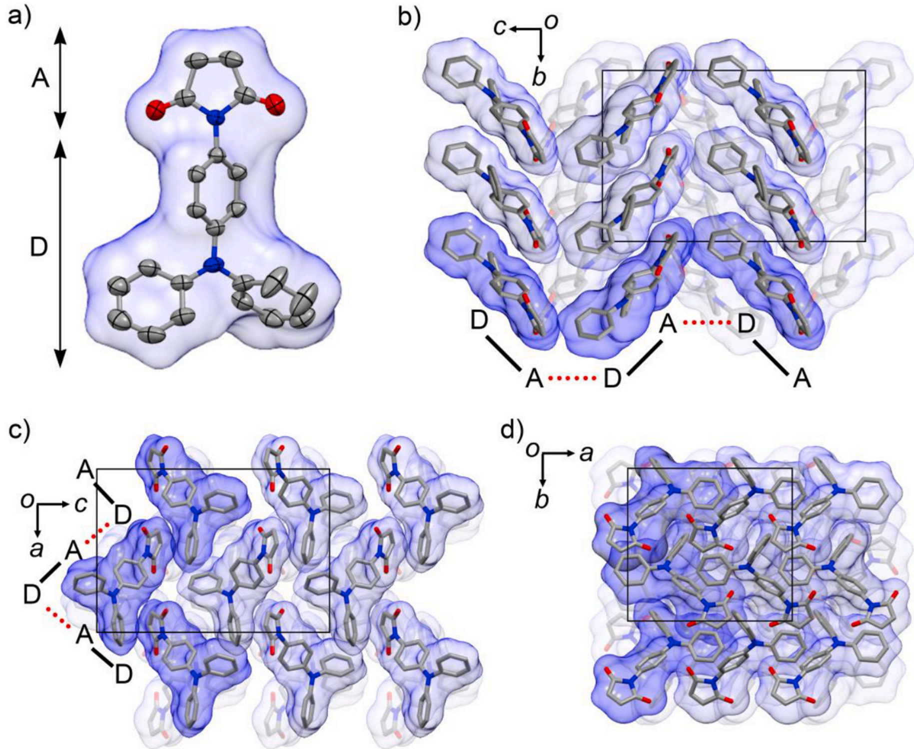

Fig. 4. a) Molecular structure (ORTEP) of dye **1** determined by single crystal X-ray diffraction. Thermal ellipsoids are drawn at 50% probability level. Crystal packing diagrams of dye **1** along the *a*-axis (b), along the *b*-axis (c) and along the *c*-axis (d). Intermolecular donor-acceptor dipole interactions are indicated by red dotted lines in (b) and (c). (For interpretation of the references to colour in this figure legend, the reader is referred to the Web version of this article.)

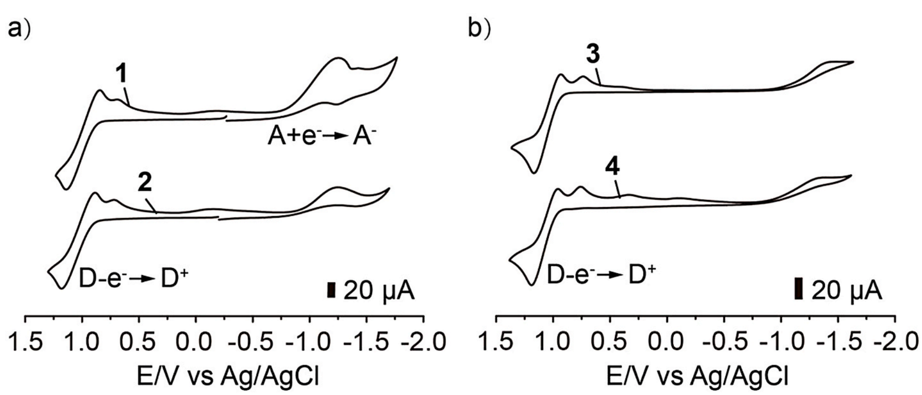

Fig. 5. a) Cyclic voltammograms of dyes **1** and **2**, $c = 0.005$ M; b) Cyclic voltammograms of dyes **3** and **4**, $c = 0.005$ M. Solvent: dichloromethane (0.1 M Bu_4NBF_6), Scanning rate: 100 mVs^{-1} (25 °C).

Table 2
Redox potentials of donors and acceptors (E_{ox}(D), E_{red}(A)), highest occupied molecular orbital (E_{HOMO}) and lowest unoccupied molecular orbital (E_{LUMO}) energy levels, energy gaps ($\Delta E_g = E_{LUMO}$-E_{HOMO}), excitation energy of donor (E_{00}(D*)), photo-induced charge transfer free energy change (ΔG) of the dyes **1**–**4**.

Dyes	E_{ox}(D)/V	E_{red}(A)/V	E_{HOMO}[b]/eV	E_{LUMO}[b]/eV	ΔE_g/eV	E_{00}(D*)/eV	ΔG/eV
1	1.14	−1.25	−5.45	−3.06	2.39	3.32	−0.99
2	1.18	−1.24	−5.49	−3.07	2.42	3.26	−0.90
3	1.17	a	−5.48	−1.73	3.75	3.32	a
4	1.19	a	−5.50	−1.73	3.77	3.32	a

[a] No data was obtained due to reduction potentials beyond the electrochemical measurement windows.
[b] Determined from cyclic voltammetry measurements. $E_{HOMO} = -[4.78\ \text{eV} + E_{ox}\ (D) - E_{Fc/Fc+}]$, $E_{LOMO} = -[4.78\ \text{eV} + E_{red}\ (A) - E_{Fc/Fc+}]$, in which $E_{Fc/Fc+}$ is the oxidation potential of ferrocene.

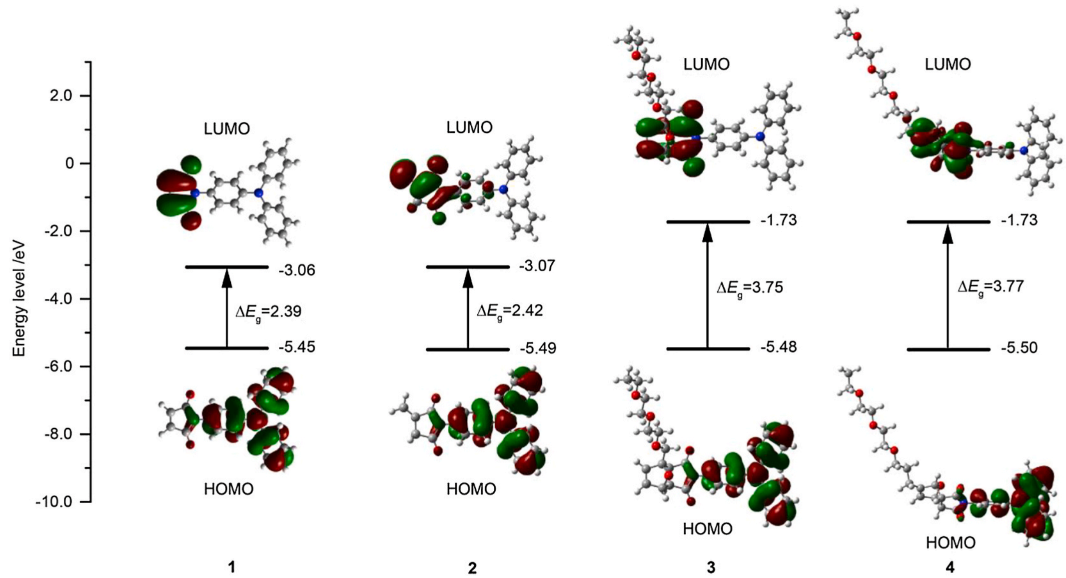

Fig. 6. Energy levels of HOMO and LUMO, energy gaps (ΔE_g), and electron cloud distribution of dyes **1**–**4** obtained by electrochemical CV measurements.

interaction [46]. The detailed crystal structure packing data of **1** were provided in Supporting Information (Table S2).

3.2. Electrochemical properties

To investigate the donor-acceptor interaction of the driving force of molecular assembly, we performed electrochemical cyclic voltammetry (CV) measurements. All these dyes show reversible oxidation peaks of triphenylamine donors at 1.14–1.19 V (Fig. 5). Dyes **1** and **2** display the irreversible reduction peaks of acceptors at −1.25 V (Fig. 5a). The relative low reduction potentials of maleimide and itaconimide acceptors suggest that they both possess an electron-accepting ability. For dyes **3** and **4,** the reduction potentials of acceptors are calculated to be −2.55 V by molecular frontier orbital calculations, which is beyond the electrochemical measurement windows (−2 V–2 V) of solvent dichloromethane. Thus, their reduction peaks are not shown in cyclic voltammograms (Fig. 5b). The electrochemical data of these dyes **1**–**4** were listed in Table 2.

On the basis of the oxidation and reduction potentials of these dyes obtained from electrochemical CV measurements, we thus obtained the highest occupied molecular orbital (E_{HOMO}) and the lowest unoccupied molecular orbital (E_{LUMO}) energy levels (Table 2 and Fig. 6). The HOMO and LUMO energy levels are closely related to ionization potential and electron affinity, which determine the chemical stability of these dyes. The energy gap ΔE_g between HOMO and LUMO energy levels is a significant parameter in determining the molecular stability and the electron transport property. In general, a small energy gap ΔE_g implies the molecule possesses a strong polarity with a high chemical reactivity and a low kinetic stability.

The HOMO energy levels of dyes **1**–**4** show approximate values due to the same triphenylamine donors they possess, while, the LUMO energy levels are quite different. LUMO energy levels of dye **1** and dye **2** are relative low, thus, the HOMO and LUMO energy gap (ΔE_g) of dye **1** and dye **2** are small enough for the formation of charge transfer state. This result further give reasonable interpretation for completely fluorescence quenching of dye **1** by intramolecular donor-to-acceptor charge transfer. Adducts **3** and **4** both possess high LUMO values indicating that electron affinity of acceptor is very weak. Thus, charge transfer interaction is weak for dyes **3** and **4**. HOMO and LUMO distributions of all dyes **1**–**4** are segregative (Fig. 6). The HOMO orbitals are mainly distributed in electron-rich triphenylamine chromophores, while, the LUMO orbitals are distributed in acceptors. The segregative

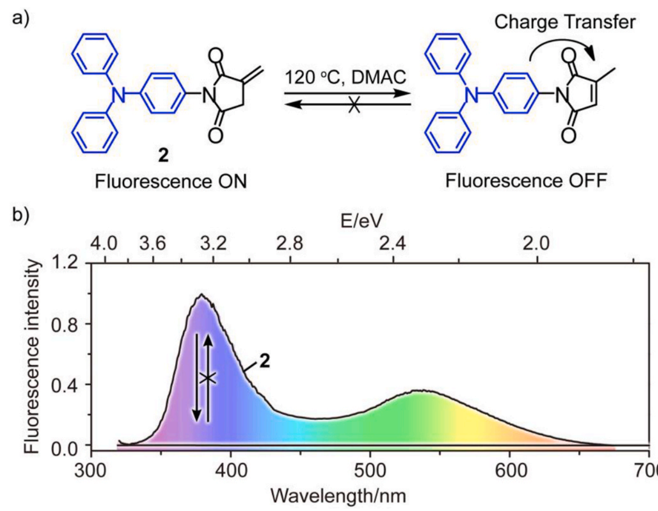

Fig. 7. Irreversible emission ON/OFF behaviours for isomerization of dye **2**. a) Isomerization of dye **2**. Reagents and conditions: *N,N*-dimethyl acetamide (DMAC), 120 °C, 3h. b) Fluorescence spectra in dichloromethane before and after isomerization of dye **2** in 1, 2-dichloroethane, [**2**] = 5×10^{-5} M, $\lambda_{ex} = 310$ nm.

characteristic of dyes **1** and **2**, and their strong acceptor suggest that charge transfer interactions are relatively strong in **1** and **2** [47]. The detailed measurement data were summarized in Table 2.

Rehm-Weller equation is usually used to estimate the charge transfer ability of donor-acceptor molecules [48,49]. The free energy change of charge transfer (ΔG) of these dyes were calculated by using Rehm-Weller equation (1):

$$\Delta G = E_{ox}(\mathrm{D})\text{-}E_{red}(\mathrm{A})\text{-}E_{00}(\mathrm{D}^*)\text{-}C \tag{1}$$

where, E_{ox}(D) and E_{red}(A) are the redox potentials of the electron donor (D) and acceptor (A), respectively; E_{00}(D*) is the energy of the 0-0 transition of the lowest excited state of the triphenylamine donor; C is stabilization energy of solvents acting with ions (0.06 eV or 1.4 kcal/mol). The negative or positive value of ΔG is regarded as a significant parameter to judge if the photo-induced charge transfer can occur [50]. The ΔG data of dyes **1** and **2** were calculated and summarized in Table 2.

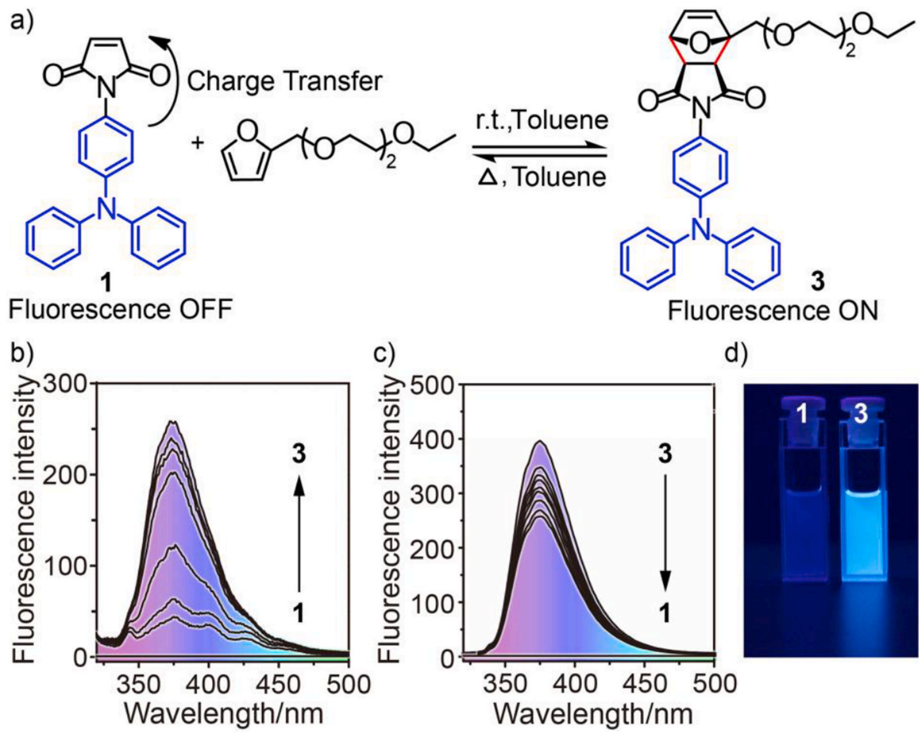

Fig. 8. Reversible emission switch ON/OFF for mutual conversion between dyes **1** and **3** by reversible Diels-Alder reaction. a) Reversible Diels-Alder addition from dye **1** to dye **3.** b) Emission spectra during Diels-Alder reaction from dye **1** to **3** in toluene: 0, 5, 10, 20, 30, 40, 50 and 60 h from bottom to top, respectively; $c = 1.1 \times 10^{-5}$ M, $\lambda_{ex} = 310$ nm. c) Emission spectra during *retro*-Diels-Alder reaction from dye **3** to **1** in toluene: 1, 2, 3, 4, 6, 8, 10, 12 and 72 h from top to bottom, respectively; $c = 1.1 \times 10^{-5}$ M, $\lambda_{ex} = 310$ nm. d) Photograph of the dichloromethane solution of dyes **1** and **3** under ultraviolet lamp (365 nm); $c = 0.1$ M.

Dyes **1** and **2** both show negative Δ*G* value, revealing that photo-induced charge transfer can occur in dyes **1** and **2**.

3.3. Dynamic dye systems with switchable ON/OFF emission

In *N*,*N*-dimethyl acetamide (DMAC) at 120 °C for 3 h, itaconimide acceptor of dye **2** is isomerized into more stable citraconimide (methyl maleimide), which is a stronger acceptor (Fig. 7a). After the itaconimide isomerization, the fluorescence was found to be completely quenched (Fig. 7a and b). This can be reasonably explained from the charge transfer quenching. The citraconimide acceptor has a stronger electron-accepting ability than itaconimide acceptor. Therefore, the charge transfer interaction becomes stronger after isomerization, which leads to a significant fluorescence quenching. For the isomerization reaction of dye **2**, the fluorescence was switched from ON to OFF (Fig. 7b). However, the emission ON/OFF is irreversible because isomerization reaction is irreversible. More stable citraconimide acceptor cannot be converted back into itaconimide acceptor.

The irreversible fluorescence isomerization is interesting, while, the reversible fluorescence switch reaction is more attractive. The single bond strength between diene and dienophile of the Diels-Alder adduct is much lower than normal covalent single bonds [51], which readily leads to a *retro*-Diels-Alder addition occurring at an elevated temperature. Therefore, an attractive characteristic of this Diels-Alder reaction is its thermal reversibility. Dye **1** was reacted with a furan derivative (2-{2-[2-(ethoxy)ethoxy]ethoxy}methyl-furan) at ambient temperature to give adduct **3** (Fig. 8a). Before the Diels-Alder addition, no fluorescence could be observable for this system, where the fluorescence of triphenylamine chromophore was completely quenched. After the Diels-Alder addition, the double bond acceptor that can quench fluorescence was consumed (Fig. 8a). Therefore, as the forward reaction proceeds, the fluorescence appears, and is turned ON (Fig. 8b). Interestingly, the emission behaviour is reversible. When the Diels-Alder adduct dye **3** was heated to 75 °C in toluene, a *retro*-Diels-Alder addition occurred according to ^{1}H NMR spectroscopy (Supporting Information Fig. S7). In this case, electron-accepting double bond was formed again. The fluorescence was gradually quenched, and switched from ON to OFF as the backward reaction proceeds (Fig. 8c). Therefore, Diels-Alder addition is a fluorescence turn ON reaction, and *retro*-Diels-Alder addition is a fluorescence turn OFF reaction. A reversible emission switch ON/OFF was observed for the thermally reversible Diels-Alder reaction. Recently, several classes of photo-induced charge transfer dye molecules have been reported including crown ether, anthracene, and pyrazoline derivatives for the detection of protons, metal ions, and reactive oxygen et al. [52–54]. Most of the data storage are inerasable because of irreversible emission properties. Our reversible emission properties based on dynamic reaction provide a valuable guideline for the rational design of a new class of fluorescence switches and development of erasable data storage devices.

To reveal dynamic dye characteristics, we performed dynamic furan exchange reaction in acetonitrile-d_3 (CD_3CN) at 75 °C. The dynamic reaction process was monitored by ^{1}H NMR spectroscopy (Fig. 9). As the reaction proceeds, the ^{1}H NMR peaks of **3** at δ 6.55–6.64 ($H_{e, f}$), δ 5.35 (H_g), δ 4.27–4.33 (H_h) and δ 3.93–4.00 ppm (H_i) and α-position furan substitution of **3** at δ 6.28 ppm (H_b) gradually decrease. Meanwhile, the ^{1}H NMR peaks of the protons of **4** at δ 5.12 ($H_{a'}$), δ 6.09 ($H_{b'}$), δ 5.30 ($H_{d'}$) and δ 4.50 ppm ($H_{j'}$) and β-position furan substitution of **4** at δ 6.30–6.36 ppm ($H_{e', f'}$) gradually appear and increase as the dynamic exchange reaction proceeds. These results reveal that β-position furan chain is more competitive than α-position furan chain in dynamic exchange reaction, where β-position furan chain has reducing steric hindrance and optimizing spatial configuration. α-position furan chain of **3** was finally replaced by β-position furan chain, thus converted into dye **4** by furan moiety exchanges (Fig. 9). The dynamic characteristic of the dye reaction enables furan exchange continuously under thermodynamic equilibrium condition to form energy-minimized and optimized molecular structures.

4. Conclusion

In summary, four triphenylamine-based dyes were synthesized by Diels-Alder cycloadditions. The studies on the optical and electrochemical properties of these dyes revealed the mechanisms of their fluorescence switches. Isomerization reaction of itaconimide dye is

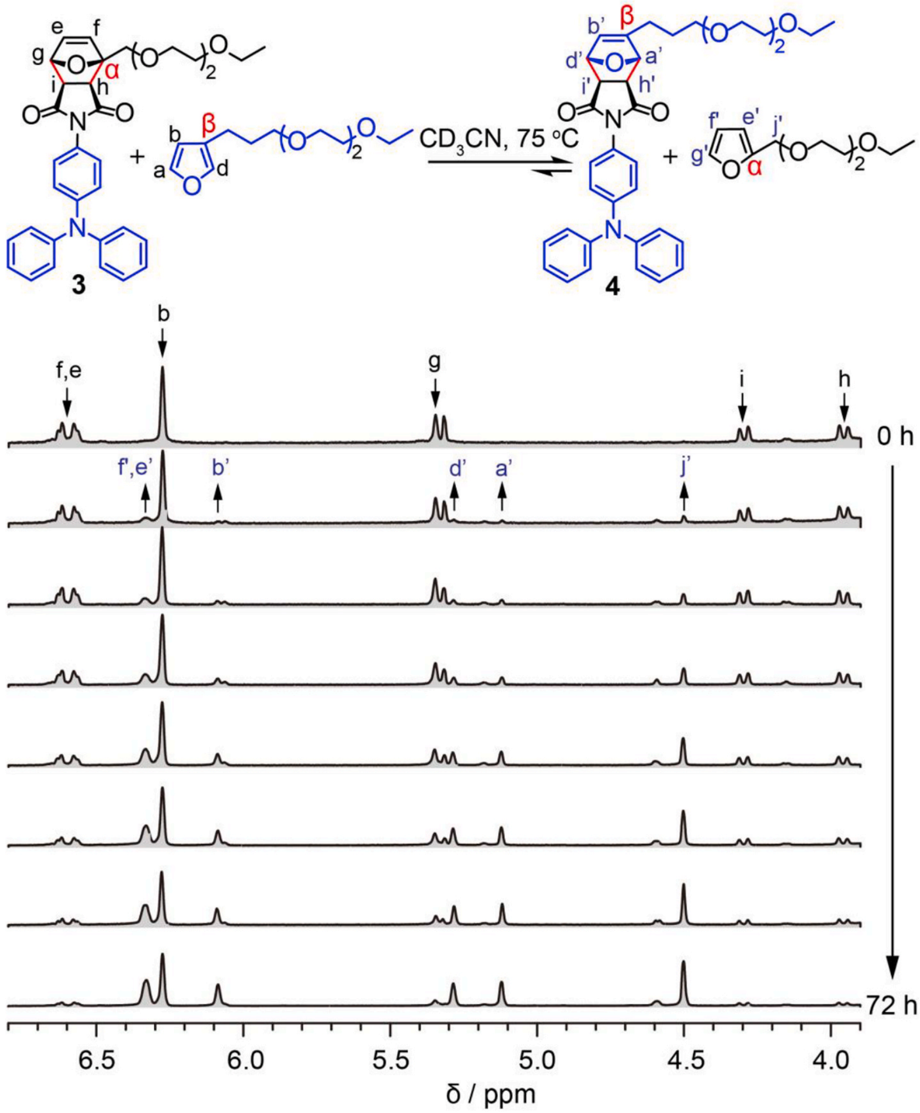

Fig. 9. Dynamic furan moiety exchanges during the conversion of α-position furan-substituted dye **3** into β-position dye **4** monitored by ^{1}H NMR spectroscopy . [**3**] = 0.05 M. Reaction time are 0, 3, 6, 12, 24, 36, 48 and 72 h from top to bottom, respectively.

irreversible, which leads to an irreversible emission turn OFF behaviours. Diels-Alder reactions of these dyes are reversible, which leads to a reversible emission turn OFF/ON behaviours. Furthermore, we demonstrate the dynamic dye systems of furan moiety exchanges based on dynamic emission turn ON reactions, where dye molecules were mutually converted, and energy-minimized, more stable, optimized molecular structure was finally formed. Our results presented here may encourage the effort for development of dynamic light-emitting dye systems and their potential applications for self-healing, recyclable, renewable materials as well as erasable data storage devices.

CRediT authorship contribution statement

Qi Zhang: Data curation, Formal analysis, Investigation. **Ying Wang:** Investigation, Methodology, Writing - original draft. **Junbo Gong:** Conceptualization, Funding acquisition, Project administration, Supervision. **Xin Zhang:** Conceptualization, Supervision, Writing - review & editing.

Declaration of competing interest

The authors declare that they have no known competing financial interests or personal relationships that could have appeared to influence the work reported in this paper.

Acknowledgements

National Natural Science Foundation of China (grant number 21674079 and 21975177) is acknowledged for financial support.

Appendix A. Supplementary data

The supporting information is available free of charge on website. Experimental procedures, synthesis, NMR spectra and HRMS of dyes **2, 3, 4** (PDF). X-ray crystallographic data of dye **1** (CIF).

Supplementary data to this article can be found online at https://doi.org/10.1016/j.dyepig.2020.108652.

References

[1] Jin Y, Yu C, Denman RJ, Zhang W. Recent advances in dynamic covalent chemistry. Chem Soc Rev 2013;42:6634–54.

[2] Jin YH, Wang Q, Taynton P, Zhang W. Dynamic covalent chemistry approaches toward macrocycles, molecular cages, and polymers. Accounts Chem Res 2014;47:1575–86.

[3] He PP, Li XD, Wang L, Wang H. Bispyrene-based self-assembled nanomaterials: in vivo self-assembly, transformation, and biomedical effects. Accounts Chem Res 2019;52:367–78.

[4] Xie N-H, Li C, Chen Y, Chen T, Liu Z, Zhu M-Q. Photoswitchable self-assembly/disassembly of near-infrared fluorophores. Chem Eur J 2018;24:16251–6.

[5] Lee S, Yang A, Moneypenny II TP, Moore JS. Kinetically trapped tetrahedral cages via alkyne metathesis. J Am Chem Soc 2016;138:2182–5.

[6] Uemura S, Sengupta S, Würthner F. Cyclic self-assembled structures of chlorophyll dyes on Hopg by the dendron wedge effect. Angew Chem Int Ed 2009;48:7825–8.

[7] Hua QX, Xin B, Xiong ZJ, Gong WL, Li C, Huang ZL, Zhu MQ. Super-resolution imaging of self-assembly of amphiphilic photoswitchable macrocycles. Chem Commun 2017;53:2669–72.

[8] Pal DS, Kar H, Ghosh S. Controllable supramolecular polymerization via a chain-growth mechanism. Chem Commun 2018;54:928–31.

[9] Ghosh G, Ghosh S. Solvent dependent pathway complexity and seeded supramolecular polymerization. Chem Commun 2018;54:5720–3.

[10] Chakma P, Konkolewicz D. Dynamic covalent bonds in polymeric materials. Angew Chem Int Ed 2019;58:9682–95.

[11] Ni C, Zha D, Ye H, Hai Y, Zhou Y, Anslyn EV, You L. Dynamic covalent chemistry within biphenyl scaffolds: reversible covalent bonding, control of selectivity, and chirality sensing with a single system. Angew Chem Int Ed 2018;57:1300–5.

[12] Tozawa T, Jones JTA, Swamy SI, Jiang S, Adams DJ, Shakespeare S, Clowes R, Bradshaw D, Hasell T, Chong SY, Tang C, Thompson S, Parker J, Trewin A, Bacsa J, Slawin AMZ, Steiner A, Cooper AI. Porous organic cages. Nat Mater 2009;8:973–8.

[13] Zou W, Dong J, Luo Y, Zhao Q, Xie T. Dynamic covalent polymer networks: from old chemistry to modern day innovations. Adv Mater 2017;29:1606100.

[14] Ying H, Zhang Y, Cheng J. Dynamic urea bond for the design of reversible and self-healing polymers. Nat Commun 2014;5:3218.

[15] Lukin O, Muller WM, Muller U, Kaufmann A, Schmidt C, Leszczynski J, Vogtle F. Covalent chemistry and conformational dynamics of topologically chiral amide-based molecular knots. Chem Eur J 2003;9:3507–17.

[16] Beuerle F, Gole B. Covalent organic frameworks and cage compounds: design and applications of polymeric and discrete organic scaffolds. Angew Chem Int Ed 2018;57:4850–78.

[17] Thote J, Aiyappa HB, Kumar RR, Kandambeth S, Biswal BP, Shinde DB, Roy NC, Banerjee R. Constructing covalent organic frameworks in water via dynamic covalent bonding. IUCrJ 2016;3:402–7.

[18] Reuther JF, Dahlhauser SD, Anslyn EV. Tunable orthogonal reversible covalent (TORC) bonds: dynamic chemical control over molecular assembly. Angew Chem Int Ed 2019;58:74–85.

[19] Jin Y, Voss BA, Noble RD, Zhang W. A shape-persistent organic molecular cage with high selectivity for the adsorption of CO_2 over N_2. Angew Chem Int Ed 2010;49:6348–51.

[20] Zhang C, Wang Q, Long H, Zhang W. A highly C_{70} selective shape-persistent rectangular prism constructed through one-step alkyne metathesis. J Am Chem Soc 2011;133:20995–1001.

[21] Okochi KD, Jin Y, Zhang W. Highly efficient one-pot synthesis of hetero-sequenced shape-persistent macrocycles through orthogonal dynamic covalent chemistry (ODCC). Chem Commun 2013;49:4418–20.

[22] Okochi KD, Han GS, Aldridge IM, Liu Y, Zhang W. Covalent assembly of heterosequenced macrocycles and molecular cages through orthogonal dynamic covalent chemistry (ODCC). Org Lett 2013;15:4296–9.

[23] Wang ZH, Gangarapu S, Escorihuela J, Fei GX, Zuilhof H, Xia HS. Dynamic covalent urea bonds and their potential for development of self-healing polymer materials. J Mater Chem 2019;7:15933–43.

[24] Dahlke J, Zechel S, Hager MD, Schubert US. How to design a self-healing polymer: general concepts of dynamic covalent bonds and their application for intrinsic healable materials. Adv Mater Interfaces 2018:180051.

[25] Zhang ZP, Rong MZ, Zhang MQ. Polymer engineering based on reversible covalent chemistry: a promising innovative pathway towards new materials and new functionalities. Prog Polym Sci 2018;80:39–93.

[26] Buryak A, Severin K. Dynamic combinatorial libraries of dye complexes as sensors. Angew Chem Int Ed 2005;44:7935–8.

[27] Bull SD, Davidson MG, Van den Elsen JMH, Fossey JS, Jenkins ATA, Jiang Y-B, et al. Exploiting the reversible covalent bonding of boronic acids: recognition, sensing, and assembly. Accounts Chem Res 2013;46:312–26.

[28] Brooks WLA, Sumerlin BS. Synthesis and applications of boronic acid-containing polymers: from materials to medicine. Chem Rev 2016;116:1375–97.

[29] Zhu LJ, Zhang YB. Crystallization of covalent organic frameworks for gas storage applications. Molecules 2017;22:1149.

[30] Jiang S, Jones JTA, Hasell T, Blythe CE, Adams DJ, Trewin A, Cooper AI. Porous organic molecular solids by dynamic covalent scrambling. Nat Commun 2011;2:207.

[31] Jin Y, Lei Z, Taynton P, Huang S, Zhang W. Malleable and recyclable thermosets: the next generation of plastics. Matter 2019;1:1456–93.

[32] Yang Y, Terentjev EM, Zhang Y, Chen Q, Zhao Y, Wei Y, Ji Y. Reprocess Therm Soft Actuator Angew Chem Int Ed 2019;58:17474–9.

[33] Sun H, Kabb CP, Dai Y, Hill MR, Ghiviriga I, Bapat AP, Sumerlin BS. Macromolecular metamorphosis via stimulus-induced transformations of polymer architecture. Nat Chem 2017;9:817–23.

[34] Gandini A. The furan/maleimide Diels-Alder reaction: a versatile click-unclick tool in macromolecular synthesis. Prog Polym Sci 2013;38:1–29.

[35] Roy N, Bruchmann B, Lehn J-M. Dynamers: dynamic polymers as self-healing materials. Chem Soc Rev 2015;44:3786–807.

[36] Li F, Li XH, Wang Y, Zhang X. Trismaleimide dendrimers: helix-to-superhelix supramolecular transition accompanied by white-light emission. Angew Chem Int Ed 2019;58:17994–8002.

[37] Ambili RV, Sasikumar D, Hridya P, Hariharan M. Deciphering the multifarious charge-transport behaviour of crystalline propeller-shaped triphenylamine analogues. Chem Eur J 2019;25:1992–2002.

[38] Hattori Y, Michail E, Schmiedel A, Moos M, Holzapfel M, Krummenacher I, Braunschweig H, Mueller U, Pflaum J, Lambert C. Luminescent mono-, di-, and triradicals: bridging polychlorinated triarylmethyl radicals by triarylamines and triarylboranes. Chem Eur J 2019;25:15463–71.

[39] Zhang X, Li ZC, Li KB, Du FS, Li FM. Multi-maleimides bearing electron-donating chromophores: reversible fluorescence and aggregation behaviour. J Am Chem Soc 2004;126:12200–1.

[40] Li F, Li XH, Zhang X. Dynamic Diels-Alder reactions of maleimide-furan amphiphiles and their fluorescence ON/OFF behaviours. Org Biomol Chem 2018;16:7871–7.

[41] Chen W-C, Yuan Y, Wu G-F, Wei H-X, Ye J, Chen M, Lu F, Tong Q-X, Wong F-L, Lee C-S. Molecular modification on bisphenanthroimidazole derivative for deep-blue organic electroluminescent material with ambipolar property and high performance. Org Electron 2015;17:159–66.

[42] Tagare J, Dubey DK, Jou JH, Vaidyanathan S. Synthesis, photophysical, theoretical and electroluminescence study of triphenylamine-imidazole based blue fluorophores for solution-processed organic light emitting diodes. Dyes Pigments 2019;160:944–56.

[43] Krijnen B, Beverloo HB, Verhoeven JW, Reiss CA, Goubitz K, Heijdenrijk D. Effect of through-bond interaction on conformation and structure of some N-arylpiperidone and N-aryltropanone derivatives. 2. ChemInform 1989;20:4433–40.

[44] Min Y, Dou CD, Liu D, Dong HL, Liu J. Quadruply B <- N-fused dibenzo-azaacene with high electron affinity and high electron mobility. J Am Chem Soc 2019;141:17015–21.

[45] Crystallographic data for **1**: 0.4 × 0.27 × 0.2 mm, orthohombic, $a = 13.899$ Å, $b = 12.908$ Å, $c = 29.765$ Å, $\alpha = 90°$, $\beta = 90°$, $\gamma = 90°$, V = 3546.2 Å 3, space group *Pbca*, Z = 8, $\rho_{calcd} = 1.275$ g cm^{-3}, λ(MoKα) = 0.71073 Å, T = 293 K, 20,569 reflections, 3130 unique [$R_{(int)} = 0.0795$], $R_1 = 0.0782$, $wR_2 = 0.0734$, for 236 parameters and 0 restraints. The X-ray single crystal data was deposited with the Cambridge Crystallographic Data Centre (CCDC 1997644).

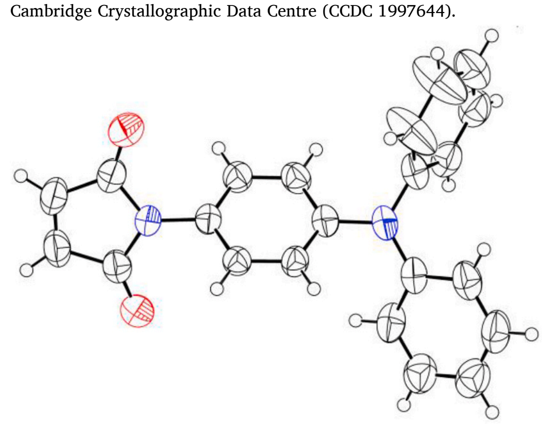

[46] Yu SS, Yang YT, Chen T, Xu JZ, Jin LY. Donor-acceptor interaction-driven self-assembly of amphiphilic rod-coil molecules into supramolecular nanoassemblies. Nanoscale 2017;9:17975–82.

[47] Chen C, Cheng M, Ding X, Li H, Qiao F, Xu L, Li H, Li H. Molecular engineering of triphenylamine functionalized phenoxazine sensitizers for highly efficient solid-state dye sensitized solar cells. Dyes Pigments 2019;162:606–10.

[48] Rehm D, Weller A. Kinetic and mechanism of electron transition for fluorescence quenching in acetonitrile. Phys Chem 1969;73:834–9.

[49] Rehm D, Weller A. Kinetics of fluorescence quenching by electron and H-atom transfer. Isr J Chem 1970;8:259–71.

[50] Sekaran B, Jang Y, Misra R, D'Souza F. Push-pull porphyrins via beta-pyrrole functionalization: evidence of excited state events leading to high-potential charge-separated states. Chem Eur J 2019;25:12991–3001.

[51] Gousse C, Gandini A. Diels-Alder polymerization of difurans with bismaleimides. Polym Int 1999;48:723–31.

[52] Daly B, Ling J, de Silva AP. Current developments in fluorescent PET (photoinduced electron transfer) sensors and switches. Chem Soc Rev 2015;44:4203–11.

[53] Li Q, Wang Z, Song W, Ma H, Dong J, Quan Y-Y, Ye X, Huang Z-S. A novel D-pi-A triphenylamine-based turn-on colorimetric and ratiometric fluorescence probe for cyanide detection. Dyes Pigments 2019;161:389–95.

[54] Liu X, Li A, Xu W, Ma Z, Jia X. Pressure-induced emission band separation of the hybridized local and charge transfer excited state in a TPE-based crystal. Phys Chem Chem Phys 2018;20:13249–54.